Carbohydrate Polymers 133 (2015) 605–612

Contents lists available at ScienceDirect

Carbohydrate Polymers

journal homepage: www.elsevier.com/locate/carbpol

Cellulose nanocrystals prepared via formic acid hydrolysis followed by TEMPO-mediated oxidation

Bin Li[a,b], Wenyang Xu[b], Dennis Kronlund[c], Anni Määttänen[c], Jun Liu[b], Jan-Henrik Smått[c], Jouko Peltonen[c], Stefan Willför[b], Xindong Mu[a,*], Chunlin Xu[b,**]

[a] CAS Kay Laboratory of Bio-Based Materials, Qingdao Institute of Bioenergy and Bioprocess Technology, Chinese Academy of Sciences, Qingdao 266101, China
[b] Johan Gadolin Process Centre, C/O Laboratory of Wood and Paper Chemistry, Åbo Akademi University, Turku FI-20500, Finland
[c] Laboratory of Physical Chemistry, Åbo Akademi University, Turku FI-20500, Finland

ARTICLE INFO

Article history:
Received 17 June 2015
Received in revised form 30 June 2015
Accepted 8 July 2015
Available online 15 July 2015

Keywords:
Cellulose nanocrystals
Formic acid
TEMPO oxidation
Characterization
Rheology

ABSTRACT

Cellulose nanocrystals (CNCs) as a renewable and biodegradable nanomaterial have wide application value. In this work, CNCs were extracted from bleached chemical pulp using two stages of isolation (*i.e.* formic acid (FA) hydrolysis and 2,2,6,6-tetramethyl-piperidine-1-oxyl (TEMPO) mediated oxidation) under mild conditions. In the first stage, FA was used to remove hemicellulose, swell cellulose fibers, and release CNCs. The FA could be readily recovered and reused. In the second stage, the CNCs isolated by FA were further modified by TEMPO-mediated oxidation to increase the surface charge of CNCs. It was found that the modified CNCs with more ordered crystal structure and higher surface charge had better redispersibility and higher viscosity in aqueous phase. Therefore, the modified CNCs could be more effective when used as rheology modifier in the fields of water based coating, paint, food *etc.*

1. Introduction

On earth, cellulose is the most abundant organic polymer built from superfine fibrils, and the annual production of cellulose is around 180 billion tons in nature (Sticklen, 2008). These superfine fibrils have nano-scale diameters and contain highly ordered crystalline regions and low-ordered or disordered amorphous regions. The amorphous regions are susceptible to break down, thus generating nano-scaled cellulose particles, *i.e.* cellulose nanocrystals (CNCs) (Habibi, 2014).

Due to its intrinsic nanostructure and properties (such as nano-scale dimensions, high specific surface area (150–250 g/m^2), high length-to-width ratio (up to several thousands), low density (1.6 g/cm^3), outstanding mechanical properties (*e.g.* high axial stiffness ~150 GPa), readily available, renewable, and sustainable sourcing), CNC as a promising nanomaterial has wide application potential in the fields of papermaking and water purification, paints and coatings, food and cosmetics, medicine and pharmacy, optical and electronic devices *etc.* (Huang et al., 2013; Shatkin, Wegner, Bilek, & Cowie, 2014; Jung et al., 2015).

The typical method for the isolation of CNC is to subject cellulosic materials (*e.g.* microcrystalline cellulose (MCC), bleached chemical pulp) to strong acid hydrolysis. The morphology and characteristics of the resulting CNC are highly dependent upon the acid used, preparation conditions, and the origin of the starting materials (Wang, Zhao, & Zhu, 2014). Sulfuric acid is the most commonly used acid for the preparation of CNC due to the mild reaction conditions (*i.e.* relatively low temperature (~45 °C) and short reaction time (~30 min)) and the good dispersibility of resulting products in water (Habibi, 2014). Other mineral acids such as hydrochloric, nitric, hydrobromic and phosphoric acids or their mixtures thereof have also been used in the CNC process (Habibi, Lucia, & Rojas, 2010). However, there are some issues with these strong acids used (*e.g.* the corrosion of equipment, the recovery of the acid, the large amount of water used, and over-degradation of cellulose) that need to be reconsidered. To address these problems, physical-assisted treatments (*e.g.* grinding (Jonoobi et al., 2015), ultrasonic treatment (Tang, Yang, Zhang, & Zhang, 2014), and steam explosion (Cherian et al., 2010)), or enzyme-assisted methods (Filson, Dawson-Andoh, & Schwegler-Berry, 2009) are applied. But physical approaches usually consume much energy, and enzymes are expensive and enzymatic hydrolysis is usually time-consuming

* Corresponding author. Fax: +86 532 80662723.
** Corresponding author.
E-mail addresses: muxd@qibebt.ac.cn (X. Mu), cxu@abo.fi (C. Xu).

http://dx.doi.org/10.1016/j.carbpol.2015.07.033
0144-8617/

(Tang et al., 2015). Most recently, solid acids were used to replace the strong liquid acids to manufacture CNC, because solid acids could be more easily and safely handled, cause less waste, and could be readily regenerated for reuse (Tang, Huang, Ou, Chen, & Chen, 2011). For instance, Liu et al., (2014) successfully prepared CNC from bleached wood pulp using phosphotungstic acid and the obtained CNC had good thermal stability as compared to the sulfated CNC. Yet, as the result of the limited contact between solid acid and cellulose, relatively long reaction time (about 15 to 30 h, or even longer) was also required.

Formic acid (FA, HCOOH, pKa 3.77, also called methanoic acid) is the simplest carboxylic acid with much stronger acidity (nearly ten-times higher acidity) than acetic acid (Balabin, 2009). FA has been used for the conversion of lignocellulosic biomass into fermentable sugars (Sun et al., 2007; Sun & Lin, 2010) and the fractionation of lignocelluloses (*e.g.* corn stover) for further utilization (Yu, Li et al., 2013), because it causes less corrosion compared to concentrated inorganic acids and it can be easily recovered and reused due to its low boiling point (100.8 °C). Hence, it is expected that FA could be used to prepare CNC or cellulose nanofibrils (CNFs) under controlled conditions.

2,2,6,6-Tetramethylpiperidine-1-oxyl (TEMPO) mediated oxidation method is a typical approach to prepare CNF (Isogai, Saito, & Fukuzumi, 2011) and it can also be used to modify the surface of CNC by increasing the carboxyl groups on the surface of CNC, thus making the modified CNC particles dispersed well in aqueous phase (Habibi, Chanzy, & Vignon, 2006). This is because the presence of the large amount of carboxyl groups on CNC surface generate strong electrostatic repulsion among CNC particles.

In the present work, CNCs were isolated from bleached chemical pulp by the use of FA, and then, the prepared CNCs were modified by TEMPO-mediated oxidation under mild conditions to improve the dispersibility of end product. In addition, the properties of the obtained CNC products were characterized by particle size distribution (PSD) analyzer, transmission electron microscopy (TEM), atomic force microscopy (AFM), Fourier transform infrared (FTIR), X-ray diffraction (XRD) analyses, thermal gravimetric analysis (TGA) *etc.* This study provided a facile approach to prepare CNC.

2. Experimental

2.1. Materials

The bleached chemical pulp (birch (*Betula pendula*)) was a gift from UPM (Finland), and the pulp samples contained 80.2 ± 0.3 wt% cellulose, 19.6 ± 0.6 wt% hemicellulose, and trace levels (less than 0.1 wt%) of lignin. Formic acid (98 wt%) and sodium hydrochloride solution (active chlorine 14 wt%) were purchased from VWR International LLC., and NaBr (extra pure) was obtained from Merck KGaA. Hydrochloric acid (37 wt%) was supplied by Mallinckrodt Baker, Inc., and TEMPO (2,2,6,6-tetramethylpiperidine-1-oxyl, 98 wt%) was purchased from Sigma–Aldrich (Finland). All chemicals were used as received without further purification.

2.2. Isolation of CNCs by formic acid hydrolysis

Two grams of bleached chemical pulp was added in 100 mL FA, and then vigorously agitated by a Mixstab TEFAL Swing (300 W, regular kitchen blender) for 1 min to obtain a pulp-like slurry. After that, a desired amount (varying from 0 to 3.17%, based on the total weight of acid in the mixture) of hydrochloric acid was added, and then the reaction took place in a spherical flask (250 mL) placed in an oil bath at 95 °C for 30 min with magnetic stirring at 900 rpm. Upon completion, the flask was immediately cooled down to room temperature with tap water, and the reaction mixture was centrifuged in a SORVALL R77 Plus centrifuge at 3500 rpm for 10 min. Subsequently, the supernatant (spent liquor) was collected and 1 mL spent liquor was taken for the analyses of acetic acid, furfural, and 5-hydroxymethyl furfural (HMF). FA was recovered by vacuum distillation and the recovery rate of FA was over 90%. The concentration of the recovered FA was 98.9 ± 0.2%. After distillation, the solid residue was dissolved in 100 mL distilled water, and then freeze-dried for the analyses of other sugar degradation products according to a previously reported procedure (Sundberg, Sundberg, Lillandt, & Holmbom, 1996).

After separation of the spent liquor, the gel-like residue obtained was washed by mixing with 200 mL distilled water and then centrifuged at 3500 rpm for 10 min. The washing procedure was repeated until the pH of suspensions reached about 6. At last, the obtained suspensions were stored in a cold room (4 °C) for further treatments or tests. The yields of the isolated product (named as F-CNC) could be calculated based on Eq. (1):

$$Y = \frac{C \times V}{m} \times 100\% \quad (1)$$

where Y is the yield of CNC, C and V are the solid content and the volume of the resultant CNC suspensions, and m is the oven dry weight of starting material (pulp).

2.3. Surface modification of F-CNC by TEMPO-mediated oxidation

To increase the surface charge density, F-CNC samples were modified by TEMPO-mediated oxidation (Liu, Korpinen et al., 2014). Briefly, the desired amounts of TEMPO (0.1 mmol/g-fiber) and NaBr (1 mmol/g-fiber) were dissolved in a certain volume of water, and then added in the F-CNC suspensions (the final consistency of F-CNC was 1 wt%) and stirred at 700 rpm. Subsequently, the surface modification started by dropwise adding NaClO solution (10 mmol/g-fiber) to the F-CNC suspension. The addition of NaClO was completed in the first 10 min and the total reaction time of the oxidation was 1 h. The reaction was carried out at pH 9.5 (adjusted by dropwise adding 0.5 M NaOH) at room temperature. Upon completion, the mixture was washed by an equivalent volume of ethanol and then centrifuged at 3500 rpm for 10 min. After that, the supernatant was decanted and the obtained cellulose gel was washed by de-ionized water twice using the same washing procedure as mentioned above. Finally, the modified F-CNC (named as T-CNC) suspension was stored in a cold room (4 °C) for further analyses. Carboxyl group content of CNC products was determined by conductometric titration method (Liu, Korpinen et al., 2014).

2.4. Preparation of CNC by sulfuric acid hydrolysis

For comparison, the sulfated CNC (S-CNC) suspensions were prepared by sulfuric acid hydrolysis (64 wt% H_2SO_4, 45 °C for 30 min) following the procedure reported previously (Liu et al., 2014).

2.5. Analysis and characterization

2.5.1. Quantitative analysis of acetic acid, furfural, and HMF in spent liquor

The contents of acetic acid, furfural, and HMF in spent liquors from FA hydrolysis were determined by a high performance liquid chromatography (HPLC); Agilent 1260 with UV diode array detector and refractive index detector were used. The furfural and HMF analyses were carried out using a Phenomenex Kinetex 2.6u C18 100 Å (150 mm × 4.6 mm) column. Eluent component A: water + 0.5% acetic acid; eluent component B: methanol + 0.5% acetic acid. The eluent composition gradually changed from 5% B in the beginning to 95% B at 10 min and then kept at 95% B until the

end of the run (13 min). The flow rate was 1.2 mL/min. The injection volume was 10 μL. The acetic acid analysis was carried out using a Phenomenex Synergi 4 μ hydro-RP C18 (250 mm × 4.6 mm) column. The eluent was 20 mM KH_2PO_4 buffer solution with pH value of 2.50–2.55 adjusted by 85% (w/w) H_3PO_4 and the flow rate was 1.0 mL/min. The injection volume was 20 μL. Known amounts of acetic acid (signal at 210 nm), furfural (signal at 276 nm), and HMF (signal at 284 nm), respectively, were analyzed to establish standard curves prior to the sample analyses. The samples of spent liquors were filtered through a 0.22 μm nylon filter before analyses.

2.5.2. The carbohydrate contents of spent liquors

The carbohydrate contents of the spent liquors from FA hydrolysis were analyzed by gas chromatography (GC) after methanolysis and silylation according to the previously reported procedure (Sundberg et al., 1996). GC analysis was done on a PerkinElmer AutoSystemXL instrument (Norwalk, USA) equipped with a high pressure (HP)-1 column. The temperature program used was: 100–175 °C, 4 °C/min, 175–290 °C, 12 °C/min. Injector 260 °C, detector 290 °C. Gas chromatography–mass spectroscopy (GC–MS) was done on an HP 6890-5973 GC–MSD instrument equipped with an HP-1 column. The oven temperature was set to stay at 80 °C for 0.5 min., and then increased to 300 °C at a rate of 8 °C/min.

2.5.3. Particle size distribution and zeta potential

The particle size distribution and zeta potential of CNC were analyzed by a Zetasizer Nano ZS instrument (Malvern Instruments Ltd., UK) based on dynamic light scattering. All the sample suspensions were ultrasonically treated (VWR, 45 kHz and 180 W) for 10 min before analysis, and the solid concentration of all samples was 0.3 wt%. For each sample, the measurements were conducted in triplicate and 7–14 runs were performed for each measurement. The average data was reported after repeated analyses.

2.5.4. Transmission electron microscopy (TEM)

The TEM images of CNC samples were taken in a JEM-1400 Plus TEM microscope (JEOL Ltd., Japan) with an accelerating voltage of 120 kV. Samples were prepared by dropping 20 μL aqueous CNC suspensions (NCC content 0.1 mg/mL) onto a carbon supported copper grid and then dyed by dropping 20 μL uranyl acetate (1 wt%). After 40 s of holding, the extra water was carefully removed by filter paper, and the remaining solution formed an even layer on grid. The samples were completely air dried before imaging.

2.5.5. Atomic force microscopy (AFM)

Topographical characterization of CNC samples was carried out with a Nanoscope V (Multimode™ series, Bruker) AFM in a PeakForce TappingTM mode. The images were obtained at ambient conditions (RH = 33%, T = 25 °C) using a SCANASYST-AIR cantilever (Bruker) with a spring constant of 0.406 N/m (thermal tune). Imaging was done using a peak force of 790–1150 pN, a scan speed of 0.68 s/μm, a peak force amplitude of 50 nm and a peak force frequency of 2 kHz. The scanning probe image processor (SPIPTM, Image Metrology, Denmark) software was used for processing and analysis of the AFM images. Before AFM analyses, one drop of CNC dispersion (2 mg/mL) was applied on a freshly cleaned mica and air dried at room temperature.

2.5.6. Redispersibility tests

The redispersibility tests of CNC suspensions were conducted by adding freeze-dried CNC samples into water, ethanol, and tetrahydrofuran (THF) respectively, and then checking the stability of the suspensions (5 mg/mL). All the samples were simultaneously treated by a VWR ultrasonic cleaner (45 kHz and 180 W) for 20 min and the pictures of samples were taken immediately after ultrasonic treatment and after standing for 10 min, 2 h, and 24 h, respectively.

2.5.7. Fourier transform infrared (FTIR)

FTIR analyses of pulp and CNC samples were carried out on a PerkinElmer FTIR-1000 spectrometer (USA), and the spectra were recorded in the wavenumber range of 400–4000 cm^{-1} with a resolution of 4 cm^{-1}. Before analysis, the samples were freeze-dried, and KBr pellet for each sample (the weight ratio of KBr to CNC was 100:1) was prepared.

2.5.8. X-ray diffraction (XRD) measurement

The XRD patterns of pulp and CNC samples were recorded at ambient conditions on an X-ray diffractometer (Bruker Discover D8, Germany), and the samples were prepared by pressing the freeze-dried pulp, or CNC samples into flattened sheets on a sample holder. The intensity of radial scans for each sample was recorded using a Cu Kα radiation which was generated at an operating voltage of 40 kV and a filament current of 40 mA. The range of scattering angle (2θ) was from 10 to 40° (scanning rate = 2 s/step, step size = 0.02°). The crystallinity index (CrI) of each sample was calculated using the empirical Eq. (2) and crystal size (D_{hkl}) was estimated using the Scherrer Eq. (3) (Segal, Greely, Martin, & Conrad, 1959) shown as follows:

$$\mathrm{CrI} = \frac{I_{200} - I_{\mathrm{am}}}{I_{200}} \times 100 \quad (2)$$

$$D_{hkl} = \frac{0.9\lambda}{\beta_{1/2}\cos\theta} \quad (3)$$

where I_{200} is the maximum peak intensity at lattice diffraction (2 0 0), I_{am} is the minimum intensity between planar reflections (2 0 0) and (1 1 0), D_{hkl} is the crystal dimension perpendicular to the diffracting planes with Miller indices of *hkl*, λ is the wavelength of X-ray radiation (λ = 1.5406 Å), and $\beta_{1/2}$ is the full width at half-maximum of the diffraction peaks.

2.5.9. Rheology measurements

The steady shear rheological behavior of CNC suspensions was performed on a modular compact rheometer (Physica MCR300, Anton Paar, Austria) at 25 °C. A Couette cell (inner radius Ri = 16.95 mm and outer radius Ro = 17.95 mm) was used for the tests with the shear range of 0.1–500 s^{-1}.

3. Results and discussion

3.1. Isolation of CNF from bleached birch pulp

Generally, for isolation of CNC using inorganic acid hydrolysis, the extraction yields and particle size of CNC are highly dependent on acid concentration, reaction temperature, and reaction time (Habibi et al., 2010). For instance, at the given conditions, higher acid concentration, higher temperature, or longer reaction time could induce a decrease in the CNC length (Camarero Espinosa, Kuhnt, Foster, & Weder, 2013). Because FA is weaker than the typical inorganic acid (*e.g.* H_2SO_4) and its boiling point is lower (*i.e.* 100.8 °C), a higher acid concentration (98%) and a relatively high reaction temperature (95 °C) were selected in order to extract CNC efficiently in this study.

Table 1 shows the isolation conditions and the properties of the resulting F-CNC products. As can be seen in Table 1, with 98% FA treatment (sample 7), about 70% yield of F-CNC (based on the initial weight of pulp) could be obtained after 6 h extraction at 95 °C. This yield was higher than that (15–60%) prepared by H_2SO_4 hydrolysis (Tang, Yang et al., 2014; Wang et al., 2014) and the one (30–60%) obtained by solid acid hydrolysis (Liu et al., 2014). The

Table 1
Isolation conditions and the properties of resulting F-CNC.

No.	FA (%)[a]	HCl (%)[a]	*t* (h)	Color of spent liquor	Color of CNC	Yield (%, oven dried (o.d.) pulp)	Size (nm)	Zeta potential (mV)
1	89.36	3.17	0.5	Dark	Pale	41.94 ± 1.36	888 ± 14	−5.10 ± 0.65
2	90.96	2.59	0.5	Deep brown	Pale	42.23 ± 1.57	958 ± 38	−6.23 ± 0.31
3	92.62	1.97	0.5	Deep brown	Pale	43.10 ± 0.70	1014 ± 25	−7.60 ± 0.78
4	94.35	1.34	0.5	Brown	Light pale	50.51 ± 0.67	1021 ± 19	−8.57 ± 0.06
5	96.14	0.68	0.5	Brown	White	58.91 ± 1.35	1060 ± 32	−6.90 ± 0.20
6	97.06	0.34	0.5	Light brown	White	63.97 ± 0.42	1070 ± 206	−6.70 ± 0.91
7	98.00	0	6	Yellow	White	69.56 ± 0.51	2819 ± 341	−6.70 ± 0.96
8[b]	98.90	0	6	Yellow	White	70.21 ± 0.13	2481 ± 115	−7.12 ± 0.16

[a] Based on the total weight of acid used; FA: formic acid; *t*: reaction time; all reactions were run at 95 °C.
[b] The recovered FA from the preparation of the sample 7 was used to prepare the sample 8.

Table 2
The yield of main degradation products in spent liquor after isolation of F-CNC[a].

No.	Glucose (%)	Xylose (%)	Mannose (%)	Galactose (%)	HMF (%)	Furfural (%)	Total (%)[d]
1	29.31 ± 0.73	3.28 ± 0.13	0.71 ± 0.16	0.63 ± 0.12	0.387 ± 0.033	9.77 ± 1.68	86.03
2	27.09 ± 0.93	6.41 ± 0.13	0.93 ± 0.02	0.71 ± 0.10	0.273 ± 0.007	9.73 ± 1.05	87.37
3	26.85 ± 1.04	7.51 ± 0.32	0.84 ± 0.12	0.54 ± 0.09	0.199 ± 0.011	7.91 ± 1.48	86.95
4	18.70 ± 0.41	11.64 ± 0.67	1.09 ± 0.05	0.73 ± 0.05	0.087 ± 0.007	6.49 ± 1.03	89.25
5	9.31 ± 0.21	14.56 ± 0.40	1.15 ± 0.01	0.47 ± 0.01	0.044 ± 0.006	4.23 ± 0.58	88.63
6	6.75 ± 0.07	13.65 ± 0.08	0.82 ± 0.02	0.19 ± 0.01	0.011 ± 0.002	2.98 ± 0.02	88.37
7	3.41 ± 0.09	13.51 ± 0.94	0.69 ± 0.05	0.11 ± 0.01	ND[b]	1.08 ± 1.07	88.36
8[c]	4.59 ± 0.67	14.57 ± 0.19	0.77 ± 0.03	0.14 ± 0.01	ND[b]	1.98 ± 0.54	91.26

[a] The data represented the weight percentage based on the weight of starting material (o.d. pulp).
[b] ND: Not determined. HMF: 5-hydroxymethyl furfural.
[c] The recovered FA from the preparation of the sample 7 was used to prepare the sample 8.
[d] Included the yield of F-CNC shown in Table 1.

corresponding average particle size (Z average) and zeta potential of F-CNC were about 2.8 μm and −6.7 mV, respectively. The color of spent liquor was yellow, which was due to the generation of chromophoric groups derived from degradation products of carbohydrates. This was in agreement with the fact that the yield of furfural (for the sample 7) was 1.08%, as presented in Table 2.

To increase the isolation speed of CNC and to shorten the reaction time, a small amount of HCl was added. As shown in Table 1, with the increase of HCl dosage, the color of the spent liquor changed from yellow to dark, and the color of F-CNC became pale when the dosage of HCl was over 1.34% (based on the total weight of acid). The color of F-CNC became dark when the reaction time was further increased. Also, the yield and size of the resulting F-CNC were reduced, which was due to the degradation of carbohydrates in the fibers. Correspondingly, as exhibited in Table 2, the glucose, HMF, and furfural yields increased with increasing HCl dosage. This was because both FA and HCl could effectively penetrate into the interior space of the cellulose fiber structure (Balabin, 2009), leading to an easy hydrolysis of hemicelluloses and the amorphous region (even partially crystalline region) of cellulose. Furthermore, the F-CNC (sample 8) extracted using the recovered FA had comparable properties with those of the sample 7, from which process the FA was recovered (Table 1). This verified that the recovered FA could be reused to prepare CNC. In addition, the total weight of F-CNC yield plus the yield of main degradation products in spent liquor of FA hydrolysis for each sample was in the range of 86–91% (much less than 100%), indicating that some degraded products might be re-adsorbed onto the surface of F-CNC.

3.2. Morphology and redispersibility of CNC

Although dynamic light scattering (DLS) could not give accurate measurement for rod-like materials, quantitative results could be obtained quickly. Thus, initial and rough analysis of CNC was still conducted by DLS methods in many studies (Yu, Qin et al., 2013). The particle size distribution (PSD) of CNC products is given in Fig. 1, which shows that the S-CNC isolated by sulfuric acid had a wide PSD

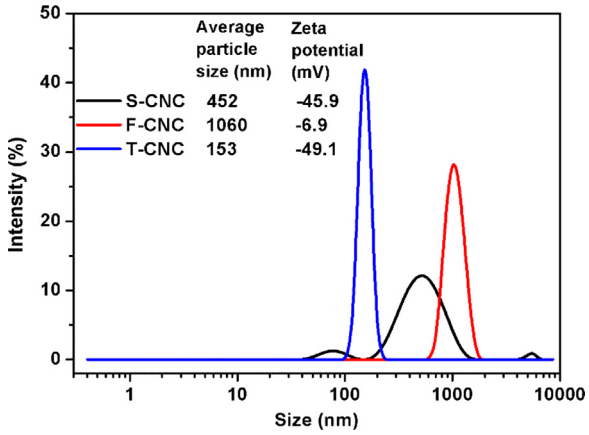

Fig. 1. Particle size distribution of CNC products (S-CNC: prepared by H_2SO_4; F-CNC (sample 5 in Table 1): prepared by FA; T-CNC: modified F-CNC by TEMPO-mediated oxidation).

(ranging from about 40 nm to 6 μm), although its average particle size was 452 nm. This was comparable with previously reported results (Sacui et al., 2014). Also, the zeta potential of S-CNC was −45.9 mV, which was associated with the presence of surface sulfate groups (Liu et al., 2014). For F-CNC (Sample 5, Table 1), its average particle size was larger (1060 nm) compared to S-CNC, but its PSD was relatively narrower ranging from about 700 nm to 1500 nm. The larger size of F-CNC obtained was due to the weaker acidity of FA and F-CNC aggregation owing to its low absolute value of the zeta potential (−6.9 mV). This was also in agreement with the fact that the polydispersity index (PDI) of F-CNC samples was 1 during PSD analysis. A PDI value of 1 indicated that the sample had a very broad size distribution or might contain large particles or aggregates that could be slowly sedimenting. The average particle size (153 nm) of T-CNC was much smaller than that of F-CNC. This was likely because of the improved dispersibility of the resulting products with much higher absolute value of zeta potential (−49.1 mV). As known, the

primary hydroxyl groups on cellulose surface could be converted to carboxyl groups during TEMPO-mediated oxidation (Isogai et al., 2011). In order to get more accurate morphology results of CNC products, TEM analyses were carried out.

Shown in Fig. 2 are the TEM images of CNC products. As can be seen, the width and length of S-CNC were in the range of 5–8 nm and 40–500 nm, respectively, and the S-CNC particles were well dispersed (Fig. 2a). Fig. 2b and c shows that the width of F-CNC was 4-6 nm, and the length of F-CNC was up to several micrometers. Also, the F-CNC was aggregated mainly due to their low absolute value of the zeta potential (Table 1). Although single F-CNC could be clearly observed, several F-CNCs were bundled together. However, after TEMPO-mediated oxidation of F-CNC, the obtained T-CNC could be well dispersed, as exhibited in Fig. 2d. The improved dispersibility of CNC (isolated using HCl) through TEMPO-mediated oxidation was also reported previously (Habibi et al., 2006). In addition, the width and length ranges of T-CNC were in 2–4 nm and 50–300 nm, respectively. These results were in good agreement with the PSD analyses shown in Fig. 1, despite the width value could not be obtained by PSD.

AFM topographical images of F-CNC and T-CNC are shown in Fig. S1a and b, respectively. It is seen in Fig. S1a that, F-CNC was strongly aggregated and formed a feather-like material, while single T-CNC particles could be well observed in Fig. S1b due to the good dispersibility in water. The height profiles along the white lines in F-CNC and T-CNC images are presented in Fig. S1c and d, respectively. Height histograms (not shown) revealed a much narrower height distribution for T-CNC compared to F-CNC. As a matter of fact, the calculated root mean square sample profile roughness (S_q value) for F-CNC and T-CNC were 16.0 nm and 2.3 nm, respectively, indicating that thinner and smoother films could be formed by T-CNC after water evaporation in comparison with F-CNC.

Because dry products are easier to be stored and transported, the full and quick redispersibility of CNC products is of crucial importance for their successful application (Liu et al., 2014). The redispersibility of S-CNC, F-CNC (sample 7), and T-CNC in water, ethanol, and tetrahydrofuran (THF) is shown in Fig. S2. It is seen that, after ultrasonic treatment, both S-CNC and F-CNC could be well re-dispersed in water, ethanol, and THF, respectively. However, F-CNC with low surface charge precipitated quickly in all the solvents used with definite precipitation and clear supernatant observed after 10 min standing. Therefore, to improve the redispersibility of F-CNC in polar or non-polar solvents, suitable surface modification should be conducted either by increasing the surface charge or by increasing the steric hindrance between the CNC particles (Habibi, 2014). Similar to S-CNC, T-CNC could be well redispersed in water, but it could not be re-dispersed well in ethanol and particularly not in THF even after 20 min ultrasonic treatment (Fig. S2). This was because T-CNC was highly negatively charged with strong hydrophilicity. Therefore, TEMPO-mediated oxidation is a suitable approach to ameliorate the redispersibility of F-CNC in aqueous phase.

3.3. Surface chemical and crystalline structure of NCC

Fig. S3 shows the FTIR spectra of bleached chemical pulp and CNC products, and the corresponding chemical band assignments of FTIR are listed in Table 3. As can be seen, the band between 3500 cm^{-1} and 3250 cm^{-1} was associated with O—H stretching, and the band at near 2900 cm^{-1} was related to the C—H stretching vibration in CH_2 groups. The small shoulder peak at 1725 cm^{-1} in the spectrum of bleached birch pulp was assigned to the C=O stretching in acetyl groups of hemicelluloses (Mou, Li, & Fardim, 2014), while in the spectrum of S-CNC the peak at 1725 cm^{-1} was absent because hemicelluloses were degraded during the sulfuric acid hydrolysis. Also, the band near 1640 cm^{-1} was ascribed to hydroxyl bending vibration of the adsorbed water (Li, Mou, Li, & Ni, 2013). In the spectrum of F-CNC (Fig. S3), there was a strong band at 1725 cm^{-1}, which was probably due to the C=O stretching in the adsorbed FA (Sun et al., 2008). It was reported that FA could be adsorbed onto the surface of cellulose by forming hydrogen bonds between FA and cellulose molecules (Sun et al., 2007; Sun & Lin, 2010). In fact, as determined, the carboxyl group content on F-CNC was 0.62 ± 0.05 mmol/g. On the other hand, it was known that FA could swell cellulose fibers and react with cellulose, generating cellulose formate (Fujimoto, Takahashi, Tsuji, Miyamoto, & Inagaki, 1986). Thus, the strong peak at around 1725 cm^{-1} was also likely and partially attributed to the C=O stretching vibration in cellulose formate. In addition, as shown in Fig. S3, in the spectrum of T-CNC, the band at 1725 cm^{-1} was related to the C=O stretching in COO—, and the band at near 1610 cm^{-1} corresponded to the antisymmetric stretching of COO— in carboxylate salts. The presence of these two bands indicated that the carboxyl groups were introduced on the T-CNC after modification of F-CNC by TEMPO-mediated oxidation (the carboxyl group content of T-CNC was 1.52 ± 0.21 mmol/g). Similar results were also reported previously (Xu, Li, Cheng, Yang, & Qin, 2014).

Table 3
Chemical band assignment of FTIR for pulp and CNC products.

Band position (cm^{-1})	Chemical band assignment
3500–3250	O—H stretching
2900	C—H stretching (CH_2)
1725	C=O stretching vibration
1640	O—H bending of absorbed water
1610	COO— (in carboxylic acid salts) antisymmetric stretching
1423	HCH and OCH in-plane bending vibration
1368	In-the-plane CH bending
1314	CH_2 rocking vibration at C6
1160	C—O—C asymmetrical stretching
897	C—O—C deformation and stretching
662	C—OH out-of-plane bending

Table 4 shows the crystallinity and crystal size of pulp and CNC products. The total crystallinity index (TCI) (Nelson & O'Connor, 1964), lateral order index (LOI) (Connor, DuPré, & Mitcham, 1958), and hydrogen-bond intensity (HBI) (Oh et al., 2005) were calculated by the FTIR absorbance ratio A_{1372}/A_{2900}, A_{1430}/A_{897}, and A_{3308}/A_{1330}, respectively. TCI, LOI, and HBI were sensitive to the crystal system and the degree of the intermolecular regularity of cellulose (Spiridon, Teacă, & Bodîrlău, 2010). The crystallinity index (CrI) and crystal size (D_{hkl}) were calculated based on the XRD determination. As can be seen in Table 4, the CrI of S-CNC increased compared to the pulp sample. This was largely due to the removal of hemicelluloses during acid hydrolysis. With respect to F-CNC, its CrI was basically unchanged (Table 4). This was likely due to the fact that FA could hydrolyze the crystalline and amorphous regions of cellulose simultaneously (Sun et al., 2008). On the other hand, the no increase of CrI for F-CNC might suggest that the amorphous materials (*i.e.* degraded hemicellulose) become re-adsorbed onto the F-CNC or bound within the immobilised water layer associated with the F-CNC surface. This was in agreement with the fact that the total yields of F-CNC and the degradation products in spent liquor of FA hydrolysis for each sample was only 86–91% (Tables 1 and 2). The CrI of T-CNC was the lowest of all, and could reflect a highly charged amorphous adsorbed layer, *i.e.* the amorphous fraction may well be preferentially carboxylated in the TEMPO oxidation. Hence, surface chemistry analysis is needed in future investigation. In comparison with the pulp sample, the increased TCI and LOI of CNC products indicated that the structure of the CNC products was more ordered (Spiridon et al., 2010). All CNC products had much higher HBI values compared to the pulp sample, indicating that more hydroxyl groups

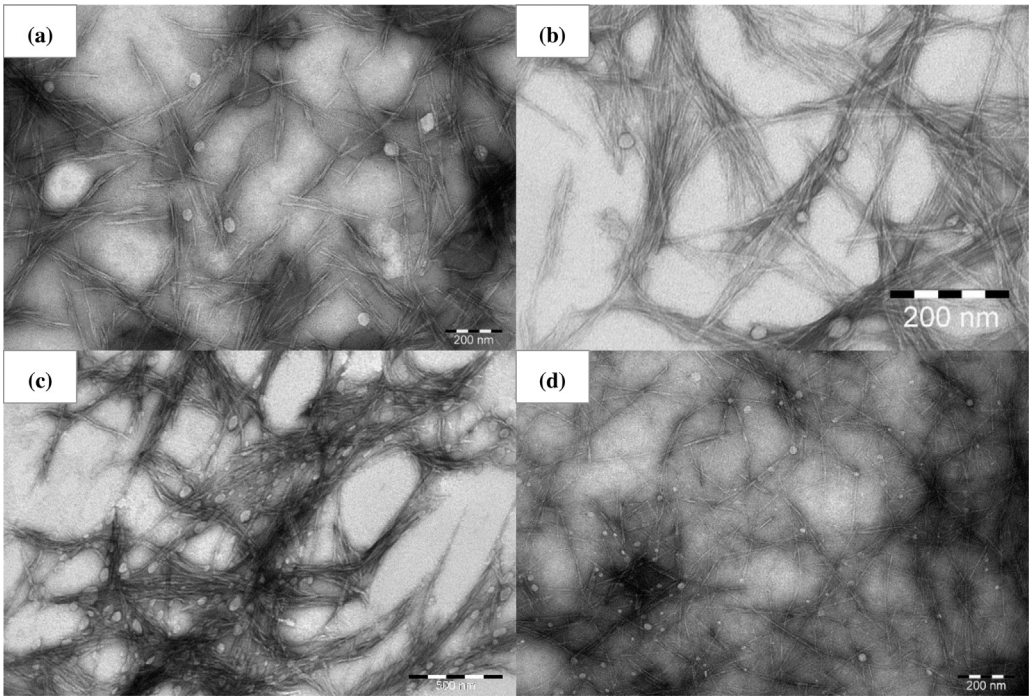

Fig. 2. TEM images of CNC products (a: S-CNC, prepared by H_2SO_4; b: F-CNC (sample 5 in Table 1), prepared by FA; c: F-CNC (sample 7 in Table 1), prepared by FA; d: T-CNC, modified F-CNC by TEMPO-mediated oxidation).

Table 4
Crystallinity and crystal size of pulp and CNC products.

Sample	TCI	LOI	HBI	CrI (%)	D_{hkl} (nm)
Pulp	1.21 ± 0.07	1.15 ± 0.02	1.87 ± 0.05	69.6 ± 0.2	5.33 ± 0.43
S-CNC	1.18 ± 0.02	1.36 ± 0.04	2.41 ± 0.03	72.4 ± 0.9	5.55 ± 0.07
F-CNC	1.41 ± 0.01	1.48 ± 0.02	2.12 ± 0.04	70.1 ± 1.7	5.62 ± 0.55
T-CNC	1.25 ± 0.03	2.10 ± 0.01	2.18 ± 0.11	67.3 ± 0.4	4.48 ± 0.01

S-NCC: Prepared by H_2SO_4; F-CNC (sample ID 7 in Table 1): prepared by FA; T-CNC: modified F-CNC by TEMPO-mediated oxidation; TCI: total crystallinity index tested by FTIR; LOI: lateral order index measured by FTIR; HBI: hydrogen-bond intensity tested by FTIR; CrI: crystallinity index analyzed by XRD; D_{hkl}: crystal planar spacing at the (2 0 0) plane calculated by XRD.

were exposed on the CNC surface, thus leading to the increased hydrogen bonding. In addition, the crystal size of F-CNC and S-CNC was a little larger than that of the pulp sample, while the crystal size of T-CNC was clearly smaller compared to the pulp sample, F-CNC and S-CNC products (Table 4).

3.4. Rheological behavior of CNC products

It is known that the rheological behavior test is of vital importance for the prediction of composites performance in the potential end applications (Urena-Benavides, Ao, Davis, & Kitchens, 2011; Yang, Tang, Wang, Kong, & Zhang, 2014) and the rheological behavior of CNC suspensions is highly related to the shear stress, solid concentration, ionic strength and the nature of CNC (*e.g.* size, surface charge density) products (Khoshkava & Kamal, 2014). In this work, the rheological behavior of CNC suspensions at the concentration of 0.3% was measured. The viscosity and shear stress as a function of shear rate are depicted in Fig. 3a and b, respectively. The shear rate was increased from 2 to 500 s^{-1}, and then continuously decreased to 2 s^{-1}. As can be seen, T-CNC suspensions displayed shear-thinning properties, *i.e.* viscosity decreased with increasing shear rate. Correspondingly, the shear stress of T-CNC suspensions increased with the increasing of shear rate (Fig. 3b). Similar results were also reported for the CNC suspensions obtained from sulfuric acid hydrolysis (Tang, He, Mosseler, & Ni, 2014). However although the viscosity of F-CNC suspension decreased when shear rate reduced in the range of 0.1–300 s^{-1}, it was nearly constant when the shear rate was higher than 300 s^{-1} (Fig. 3a). Moreover, the viscosity of the T-CNC suspension was higher than that of F-CNC at the same shear rate, as exhibited in Fig. 3a. This was because of the aggregation of F-CNC and its low charge density, resulting in a weaker interactions among the F-CNC agglomerate particles in comparison with the stronger inter-particle repulsion of the dispersed T-CNC, and this was also in agreement with the results displayed in Figs. 1, 2, S1, and S2. For S-CNC, it was known that the viscosity was CNC concentration depended, and higher sulfonation degree of CNC led to a higher viscosity of CNC suspension (Shafiei-Sabet, Hamad, & Hatzikiriakos, 2013). Therefore, it is expected that T-CNC products with higher surface carboxyl group content could be more effective to be used as a rheological modifier in the fields of waterborne coating, paints, food *etc.* compared to F-CNC, although further investigation is needed to quantify the effect of CNC concentration on viscosity and viscoelastic property.

In addition, Bingham model (expressed in Eq. (4)) could fit well the shear rate upward and downward curves of CNC suspensions, respectively.

$$\tau = \tau_0 + \eta g \tag{4}$$

where τ is shear stress and γ is shear rate; τ_0 and η are yield stress and plastic viscosity, respectively. The Bingham model represents an idealized type of flow combining yield stress and constant viscosity flow (or Newtonian flow), and the flow of suspensions occurs

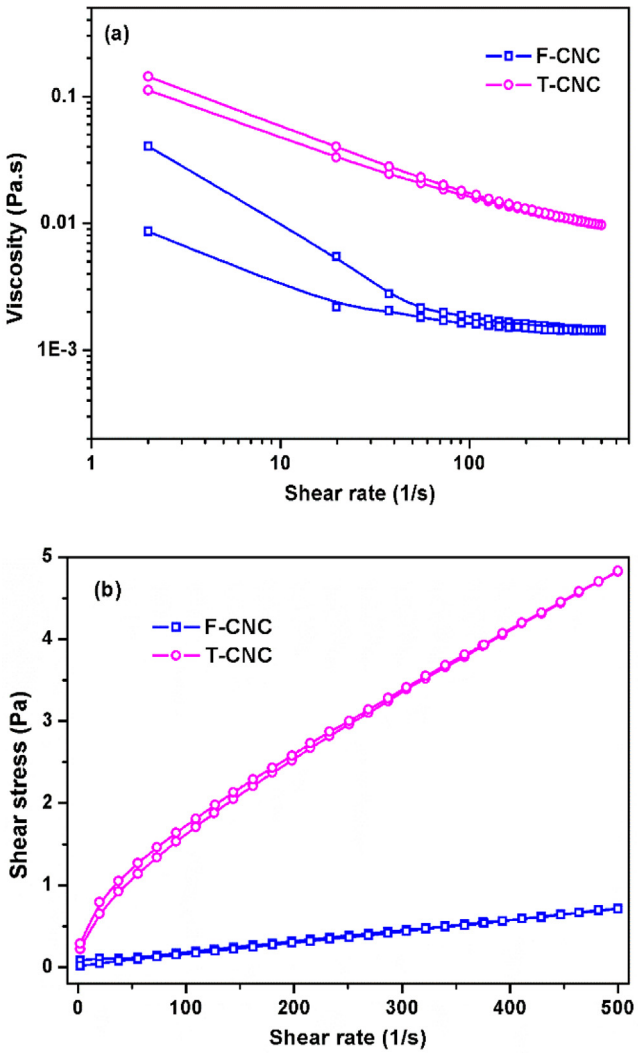

Fig. 3. Rheological behavior of CNC suspensions (a: viscosity *vs* shear rate; b: shear stress *vs* shear rate; F-CNC (sample 7 in Table 1): prepared by FA; T-CNC: modified F-CNC by TEMPO-mediated oxidation).

Table 5
Rheological parameters of Bingham model fitted to flow curves of CNC suspensions.

Sample	Yield stress (Pa)	Plastic viscosity (Pa s)
F-CNF[a]	0.0594	1.3×10^{-3}
F-CNF[b]	0.0208	1.4×10^{-3}
T-CNC[a]	0.6968	8.6×10^{-3}
T-CNC[b]	0.8164	8.3×10^{-3}

[a] Upward curve of shear rate.
[b] Downward curve of shear rate.

once the applied stress exceeds the τ_0 (Liu, Hu, Nairy, Jahan, Yang, & Ni, 2013). Shown in Table 5 is the rheological parameters of Bingham model fitted to flow curves of CNC suspensions. As can be seen, both τ_0 and η for T-CNC suspensions were obviously higher compared to F-CNC suspensions, and this was in good agreement with the results presented in Fig. 3.

4. Conclusions

In this study, a facile method was established to prepare cellulose nanocrystals (CNCs) using formic acid hydrolysis of bleached chemical pulp and the followed surface modification through TEMPO-mediated oxidation. Formic acid could be readily recovered and reused. The resultant CNCs (T-CNC) had a width of 2–4 nm and length of 50–300 nm respectively. Compared to unmodified CNC (F-CNC), T-CNC with higher surface carboxyl group content and more ordered crystalline structure had much better redispersibility and higher viscosity in aqueous phase. Thus, it could be expected that T-CNC would be more effective when used as rheological modifier in comparison with F-CNC.

Acknowledgements

We gratefully acknowledge the support from the Johan Gadolin Scholarship Programme at the Process Chemistry Centre at Åbo Akademi University (Finland). The work was also partly financially supported by the National Natural Science Foundation of China (Nos. 21306216 and 31470609) and Shandong Provincial Natural Science Foundation for Distinguish Young Scholar (China) (No. JQ201305). At last, the authors thank Mr. Jarl Hemming from the Lab. of Wood and Paper Chemistry in Åbo Akademi University for helping with the HPLC analyses, Dr. Mari Nurmi from the Lab. of Paper Coating and Converting in Åbo Akademi University for helping on the rheology tests, and Dr. Markus Peurla at Lab. of Electron Microscopy, University of Turku (Finland) for helping on the TEM measurements.

Appendix A. Supplementary data

Supplementary data associated with this article can be found, in the online version, at http://dx.doi.org/10.1016/j.carbpol.2015.07.033

References

Balabin, R. M. (2009). Polar (acyclic) isomer of formic acid dimer: gas-phase raman spectroscopy study and thermodynamic paramerters. *Journal of Physical Chemistry*, *113*, 4910–4918.
Camarero Espinosa, S., Kuhnt, T., Foster, E. J., & Weder, C. (2013). Isolation of thermally stable cellulose nanocrystals by phosphoric acid hydrolysis. *Biomaromolecules*, *14*, 1223–1230.
Cherian, B. M., Leão, A. L., de Souza, S. F., Thomas, S., Pothan, L. A., & Kottaisamy, M. (2010). Isolation of nanocellulose from pineapple leaf fibres by steam explosion. *Carbohydrate Polymers*, *81*, 720–725.
Filson, P. B., Dawson-Andoh, B. E., & Schwegler-Berry, D. (2009). Enzymatic-mediated production of cellulose nanocrystals from recycled pulp. *Green Chemistry*, *11*, 1808–1814.
Fujimoto, T., Takahashi, S. I., Tsuji, M., Miyamoto, T., & Inagaki, H. (1986). Reaction of cellulose with formic acid and stability of cellulose formate. *Journal of Polymer Science: Part C: Polymer Letters*, *24*, 495–501.
Jonoobi, M., Oladi, R., Davoudpour, Y., Oksman, K., Dufresne, A., Hamzeh, Y., et al. (2015). Different preparation methods and properties of nanostructured cellulose from various natural resources and residues: a review. *cellulose*, *22*, 935–969.
Jung, Y. H., Chang, T.-H., Zhang, H., Yao, C., Zheng, Q., Yang, V. W., et al. (2015). High-performance green flexible electronics based on biodegradable cellulose nanofibrils paper. *Nature Communications*, *6*, 7170. http://dx.doi.org/10.1038/ncomms8170
Habibi, Y. (2014). Key advances in the chemical modification of nanocelluloses. *Chemical Society Reviews*, *43*, 1519–1542.
Habibi, Y., Chanzy, H., & Vignon, M. R. (2006). TEMPO-mediated surface oxidation of cellulose whiskers. *Cellulose*, *13*, 679–687.
Habibi, Y., Lucia, L. A., & Rojas, O. J. (2010). Cellulose nanocrystals: chemistry, self-assembly, and application. *Chemical Reviews*, *110*, 3479–3500.
Huang J., Zhu H., Chen Y., Preston C., Rohrbach K., Cumings J., et al., Highly transparent and flexible nanopaper transistors. *ACS Nano*, *7*, 2013, 2106-2113.
Isogai, A., Saito, T., & Fukuzumi, H. (2011). TEMPO-oxidized cellulose nanofibers. *Nanoscale*, *3*, 71–85.
Khoshkava, V., & Kamal, M. R. (2014). Effect of cellulose nanocrystals (CNC) particle morphology on dispersion and rheological and mechanical properties of polypropylene/CNC nanocomposites. *ACS Applied Materials & Interfaces*, *6*, 8146–8157.
Li, B., Mou, H., Li, Y., & Ni, Y. (2013). Synthesis and thermal decomposition behavior of zircoaluminate coupling agents. *Industrial & Engineering Chemistry Research*, *52*, 11980–11987.
Liu, H. T., Hu, H. R., Nairy, A., Jahan, M. S., Yang, G. H., & Ni, Y. H. (2013). Viscosity of prehydrolysis liquor of a hardwood kraft-based dissolving pulp production process. *Industrial & Engineering Chemistry Research*, *52*, 3974–3979.

Liu, J., Korpinen, R., Mikkonen, K. S., Willför, S., & Xu, C. (2014). Nanofibrillated cellulose originated from birch sawdust after sequential extractions: a promising polymeric material from waste to films. *Cellulose*, *21*, 2587–2598.
Liu, Y., Wang, H., Yu, G., Yu, Q., Li, B., & Mu, X. (2014). A novel approach for the preparation of nanocrystalline cellulose by using phosphotungstic acid. *Carbohydrate Polymers*, *110*, 415–422.
Mou, H., Li, B., & Fardim, P. (2014). Pretreatment of corn stover with the modified hydrotropic method to enhance enzymatic hydrolysis. *Energy Fuels*, *28*, 4288–4293.
Nelson, M. L., & O'Connor, R. T. (1964). Relation of certain infrared bands to cellulose crystallinity and crystal lattice type. Part II. A new infrared ratio for estimation of crystallinity in celluloses I and II. *Journal of Applied Polymer Science*, *8*, 1325–1341.
O'Connor, R. T., DuPré, E. F., & Mitcham, D. (1958). Applications of infrared absorption spectroscopy to investigations of cotton and modified cottons. Part I: physical and crystalline modifications and oxidation. *Textile Research Journal*, *28*, 382–392.
Oh, S. Y., Dong, I. Y., Shin, Y., Hwan, C. K., Hak, Y. K., Yong, S. C., et al. (2005). Crystalline structure analysis of cellulose treated with sodium hydroxide and carbon dioxide by means of X-ray diffraction and FTIR spectroscopy. *Carbohydrate Research*, *340*, 2376–2391.
Sacui, I. A., Nieuwendaal, R. C., Burnett, D. J., Stranick, S. J., Jorfi, M., Weder, C., et al. (2014). Comparison of the properties of cellulose nanocrystals and cellulose nanofibrils isolated from bacteria, tunicate, and wood processed using acid, enzymatic, methanical, and oxidative methods. *ACS Applied Materials & Interface*, *6*, 6127–6138.
Segal, L., Greely, J., Martin, A., & Conrad, C. (1959). An empirical method for estimating the degree of crystallinity of native cellulose using the X-ray diffractometer. *Textile Research Journal*, *29*, 786–794.
Shafiei-Sabet, S., Hamad, W. Y., & Hatzikiriakos, S. G. (2013). Influence of degree of sulfation on the rheology of cellulose nanocrystal suspensions. *Rheologica Acta*, *52*, 741–751.
Shatkin, J. A., Wegner, T. H., Bilek, E. M., & Cowie, J. (2014). Market projections of cellulose nanomaterial-enabled products –Part 1: applications. *Tappi Journal*, *13*, 9–16.
Spiridon, I., Teacă, C.-A., & Bodîrlău, R. (2010). Structural changes evidenced by FTIR spectroscopy in cellulosic materials after pretreatment with ionic liquid and enzymatic hydrolysis. *BioResources*, *6*, 400–413.
Sticklen, M. B. (2008). Plant genetic engineering for biofuel production: towards affordable cellulosic ethanol. *Nature Review Genetics*, *9*, 433–443.
Sun, Y., & Lin, L. (2010). Hydrolysis behavior of bamboo fiber in formic acid reaction system. *Journal of Agricultural Food & Chemistry*, *58*, 2253–2259.
Sun, Y., Lin, L., Pang, C., Deng, H., Peng, H., Li, J., et al. (2007). Hydrolysis of cotton fiber cellulose in formic acid. *Energy Fuels*, *21*, 2386–2389.
Sun, Y., Lin, L., Deng, H., Li, J., He, B., Sun, R., et al. (2008). Structural changes of bamboo cellulose in formic acid. *BioResources*, *3*(2), 297–315.
Sundberg, A., Sundberg, K., Lillandt, C., & Holmbom, B. (1996). Determination of hemicelluloses and pectins in wood and pulp fibres by acid methanolysis and gas chromatography. *Nordic Pulp & Paper Research Journal*, *11*, 216–219.
Tang, Y., He, Z., Mosseler, J. A., & Ni, Y. (2014). Production of highly electro-conductive cellulosic paper via surface coating of carbon nanotube/graphene oxide nanocomposites using nanocrystalline cellulose as a binder. *Cellulose*, *21*, 4569–4581.
Tang, Y., Yang, S., Zhang, N., & Zhang, J. (2014). Preparation and characterization of nanocrystalline cellulose via low-intensity ultrasonic-assisted sulfuric acid hydrolysis. *Cellulose*, *21*, 335–346.
Tang, L., Huang, B., Ou, W., Chen, X., & Chen, Y. (2011). Manufacture of cellulose nanocrystals by cation exchange resion-catalyzed hydrolysis of cellulose. *Bioresource Technology*, *102*, 10973–10977.
Tang, Y., Shen, X., Zhang, J., Guo, D., Kong, F., & Zhang, N. (2015). Extraction of cellulose nano-crystals from old corrugated container fiber using phosphoric acid and enzymatic hydrolysis followed by sonication. *Carbohydrate Polymers*, *125*, 360–366.
Urena-Benavides, E. E., Ao, G., Davis, V. A., & Kitchens, C. L. (2011). Rheology and phase behavior of lyotropic cellulose nanocrystal suspensions. *Macromolecules*, *44*, 8990–8998.
Wang, Q., Zhao, X., & Zhu, J. Y. (2014). Kinetics of strong acid hydrolysis of a bleached kraft pulp for producing cellulose nanocrystals (CNCs). *Industrial & Engineering Chemistry Research*, *53*(27), 11007–11014.
Xu, Q., Li, W., Cheng, Z. L., Yang, G., & Qin, M. H. (2014). TEMPO/NaBr/NaClO-mediated surface oxidation of nanocrystalline cellulose and its microparticulate retention system with cationic polyacrylamide. *BioResources*, *9*(1), 994–1006.
Yang, S., Tang, Y., Wang, J., Kong, F., & Zhang, J. (2014). Surface treatment of cellulosic paper with starch-based composites reinforced with nanocrystalline cellulose. *Industrial & Engineering Chemistry Research*, *53*, 13980–13988.
Yu, G., Li, B., Liu, C., Zhang, Y., Wang, H., & Mu, X. (2013). Fractionation of the main components of corn stover by formic acid and enzymatic saccharification of solid residue. *Industrial Crops and Products*, *50*, 750–757.
Yu, H., Qin, Z., Liang, B., Liu, N., Zhou, Z., & Chen, L. (2013). Facile extraction of thermally stable cellulose nanocrystals with a high yield of 93% through hydrochloric acid hydrolysis under hydrothermal conditions. *Journal of Materials Chemistry A*, *1*, 3938–3944.